Two classes of Richtmyer-Meshkov instabilities: A detailed statistical look

J. R. Ristorcelli, A. A. Gowardhan, and F. F. Grinstein

Additional information on Phys. Fluids

Two classes of Richtmyer-Meshkov instabilities: A detailed statistical look

J. R. Ristorcelli, A. A. Gowardhan,[a)] and F. F. Grinstein
Los Alamos National Laboratory, Los Alamos, New Mexico 87545, USA

A single parameter numerical study of the evolution of the multimode planar Richtmyer-Meshkov instability (RMI) in a shocked/reshocked (air-SF$_6$, Atwood number $A = 0.67$) configuration with a Mach number $Ma = 1.5$ shock is carried out. Our results demonstrate that the initial material interface morphology (for fixed Ma, A) controls the RMI evolution characteristics. Our discussion focuses on the light-to-heavy configuration with initial $A > 0$ and heavy-to-light reshock. Depending on the *rms* slope of the initial interface, η_o, there are two different instabilities: one with the classical RMI trends and another with trends suggesting a very different fluid physics which we study in detail. We use statistical metrics to demonstrate that the two different regimes are characterized by very different and self-consistent fluid physics. The response of the rate of mixing layer growth to increasing η_o is different and opposite in sign in each regime: in the high-η_o class of initial conditions, increasing η_o leads to a decrease in kinetic energy and mixing layer growth rate; and in the low-η_o class of flows, increasing η_o leads to an increase in kinetic energy and growth rate. The low η_o case corresponds to impulsive acceleration of an almost-flat thin interface, the classical small-perturbation RMI. The high-η_o regime corresponds to: (a) impulsive acceleration of a very rough initial interface, and (b) shock passage through a turbulent material interface. We additionally observe that this bipolar behavior of the turbulent field is not seen in the statistics of the material mixing field and this may invalidate closures that slave the mixing field to the turbulence. It appears that simple Reynolds-Averaged Navier-Stokes moment closure models cannot currently predict both classes of RMI. We offer speculations on the similarity of instabilities and the possibility of using high-η_o first-shocked simulations to study reshock problems. Our article describes these two instabilities as a function of η_o for fixed A and Ma; we do not propose that η_o offers a complete parameterization of the general problem. © *2013 AIP Publishing LLC*. [http://dx.doi.org/10.1063/1.4802039]

I. INTRODUCTION

In many areas of interest such as, inertial confinement fusion (ICF), understanding the collapse of the outer cores of supernovas, vorticity is introduced at material interfaces by the impulsive loading of shock waves, and turbulence is generated via the so-called Richtmyer-Meshkov instability (RMI).[1] RMI adds the complexity of shock waves and other compressible effects such as baroclinic enstrophy generation to the basic physics associated with transition and turbulent mixing. These flows are typically investigated using the early-time relevant RMI model for a first-shocked relatively flat and thin material interface.[1] However, for most classes of shock-induced mixing, reshocks which happen at a later-time and involve morphologically more complex interfacial layers and fluid instability mechanisms distinctly different from RMI are more important phenomena; the distinction between the classical RMI and this new nonlinear instability is one major focus of the present work. Beyond

---

a)Present address: NARAC, Lawrence Livermore National Laboratory, Livermore, California 94550, USA.

the work surveyed in Ref. 1, investigation of initial condition (IC) effects on RMI has been the subject of many experimental,[2–6] numerical,[6–19] as well as theoretical[13,20] studies.

In contrast with forced isotropic homogeneous turbulence, where stable statistics are achieved, the flow we study is inherently transitional and non-equilibrium before relaxing to an inhomogeneous quasi-equilibrium decaying turbulence at long times. Nonetheless we use the same statistical methods as used in traditional studies of equilibrium turbulence to study the early time instability and transition mechanisms. A flow transition in the RMI is caused by energy from the shock interface interaction being deposited at the interfacial layer over finite periods of time during its interaction with the shock, compression, or expansion-fan waves. Transition to turbulence is traditionally viewed in terms of rapid increase in the energy and the production by mode coupling of a spectrum of smaller length scale motions which can lead to an inertial subrange in the turbulent kinetic energy spectrum for sufficiently high Reynolds number (Re),[31]e.g., above the proposed mixing-transition Taylor microscale based Re, $Re_\lambda = 100$.[32]

In the RMI simple models for the growth rates of the interfacial layer undergoing acceleration by a shock depend on the Atwood number, $A = (\rho_{inner} - \rho_{outer})/(\rho_{inner} + \rho_{outer})$, where outer denotes the gas the shock wave traverses before it impacts the material interface, the shock Mach number, Ma, and some measure of the interfacial perturbations. Layer growth rates are consistently much higher after reshock;[18] transition after reshock is typically observed[10,14,17] and extreme sensitivity to detailed conditions at reshock time has been reported.[2,14,26] Before reshock, transition has been[8,17] or not been[8,10,14] observed; transition occurrence has been reported to depend on particular combination of IC specifics such as sign and magnitude of A,[18] Ma,[6,33] and Re;[8] IC resolution issues[14] are also likely relevant in the numerical transition context. The work in Refs. 6 and 33 reports a very notable RMI growth sensitivity to Ma, particularly with regards to the transition process;[33] as little as a 15% variation in Ma can make the difference for a shocked interface to undergo or not undergo transition.

A. Preview

In this report we focus on the light-to-heavy (L-H) ($A > 0$, air/SF_6) planar shock-tube configuration, and on investigating effects of initial material interfacial morphology on the shock and the reshock problems. More specifically, we consider a stochastic initial interface with varying interfacial perturbation spectra. This is a stochastic multi-mode IC problem in which changes induced in the RMI by changes in characteristic amplitude and wavelengths of the initial interfacial are studied. Our interest in this problem is motivated by the change in the nature of the instability as the initial interfacial *rms* slope η_o is increased as first reported in our earlier work on the bipolar nature of the RMI.[21] For large η_o, what one might call a nonlinear RMI, the simulations exhibit a behavior that bears little resemblance to the trends of the well-known conventional or linear RMI.

The change of the instability mechanism is of interest in its own right on fundamental grounds. Our studies are also prompted by additional applications. The low-η_o or linear RMI case corresponds to the shock passage across an almost flat thin interface. In the literature this is, ostensibly, the most studied case. The high-η_o or what we may call the nonlinear RMI corresponds to the (a) the shock passage across a very rough interface, and (b) the shock impacting a fully turbulent interface between dissimilar materials. Our central focus is presenting a more detailed study the two classes RMI instabilities using statistical metrics not used in RMI studies. We apply metrics from statistical approaches to turbulence as well as ones derived from the second order moment equations that are used for turbulence model development to analyze the flow. There is a caveat: the application of metrics developed for stationary homogenous high Reynolds turbulence requires some caution when applied to non-stationary, non-equilibrium, inhomogeneous low Reynolds number turbulence. Our investigation is also motivated by the associated turbulence modeling challenge: are turbulence models general enough to predict both classes of the RMI—and thus complex systems involving flow with sequential shocks?

As the instability mechanism for the nonlinear RMI appears primarily due to enstrophy production by the nonlinear cascade mechanism and not baroclinicity it seems possible to speculate with our partial numerical evidence that the nonlinear RMI is the instability relevant to the RMI

reshock problem. As our studies are single parameter *rms* slope studies targeted for a specific project we have limited our studies to a single *Ma* and $A > 0$. The $A < 0$ studies necessary to formally make connections between the high *rms* slope first-shock problem and the reshock problem for arbitrary density configurations are required. An important observation in our study of the L-H ($A > 0$) configuration, is that the statistical trends of heavy-to-light (H-L) reshock effects on mixing and transition as function of η_o can be produced with a first-shocked L-H configuration if η_o is high enough. If the primary instability mechanism is the mode coupling of the cascade and the enstrophy strain feedback loop then the results we speculate on are more general. This has potential relevance to reducing computational and experimental costs to address reshocked turbulent interface research. It will be left an open question.

Our present focus is on understanding the instability and transition following first-shock (or reshock) as related to interfacial IC characteristics. Late-time asymptotic behaviors of the quasi-equilibrium decaying turbulence is not our particular interest here: they likely involve inhomogeneous turbulence decay conforming to traditional self-similar scalings with weak dependence on ICs[35] and, particularly, on the infrared portion of the initial spectrum.[36] Moreover, as is well known in the turbulence literature, simulations of the long time problem suffer from the integral scale saturation problem: when the integral scale of the turbulence becomes of the order of the computational domain (or laboratory facility) smallest characteristic size, the power laws of different decays tend to approach each other (see also Ref. 39).

B. Outline

The plan of the paper is as follows. In Sec. II the problem statement and methodology are summarized. Sections III and IV are devoted to our description of the two different classes of instability. In Sec. III we use the usual mixing layer width as a metric. In Sec. IV, we use metrics of the flow that come from the moment evolution equations for a turbulent flow and paint a very clear distinction regarding the "bipolar" responses of the instability first recognized in Ref. 21; here we look at the physics in substantially more depth using more comprehensive measures used in studies of traditional turbulent flows.[22] We offer speculations on the similarity of instabilities and the possibility of using high-η_o first-shocked simulations to study reshock problems; however, we are careful to also leave this as an open problem as H-L first-shocked simulations are not part of our present scope area. After delineating the two classes of RMI using a moment closure based narrative, we discuss how the observations of the material mixing physics are consistent with the fluid physics further consolidating a more detailed pictures of nonlinear RMI. In Sec. V we document statistics relevant to testing moment closure procedures for material mixing, and Sec. VI examines the challenges that these two classes of RMI present to turbulence models of the moment equation type. Summary and conclusions are presented in Sec. VII.

II. PROBLEM STATEMENT, SIMULATION, AND ANALYSIS METHOD

The planar shock-tube configuration investigated involves low (air) and high (SF_6) density gases, presumed ICs at the material interface initially separating the gases, and eventual reshock off an end-wall (Fig. 1). The contact discontinuity between air and SF_6 is modeled as a jump in density using ideal gases with $\gamma = 1.4$ and $\gamma = 1.076$, respectively, with constant pressure across the initial interface at rest. A shocked air region is created upstream satisfying the Rankine-Hugoniot relations for a Mach 1.5 shock. The shock propagates in the (x) direction through the contact discontinuity (from the light to heavy fluid) and reflects at the end of the simulation box on the right. Periodic boundary conditions are imposed in the transverse (y,z) directions. The air/SF_6 interface is shocked at $t = 0$, reshocked by the primary reflected shock at $t \sim 3.5$ ms, and then by successive reflected expansion and compression waves of decreasing intensity. The evolution and interaction of the shock and air/SF_6 interface (e.g., as in Fig. 1) are in good agreement with those of similar reported studies.[14]

Because shocks and turbulence are involved, resolving all relevant physical scales in RMI simulations becomes prohibitively expensive. Turbulent material mixing can be usefully characterized
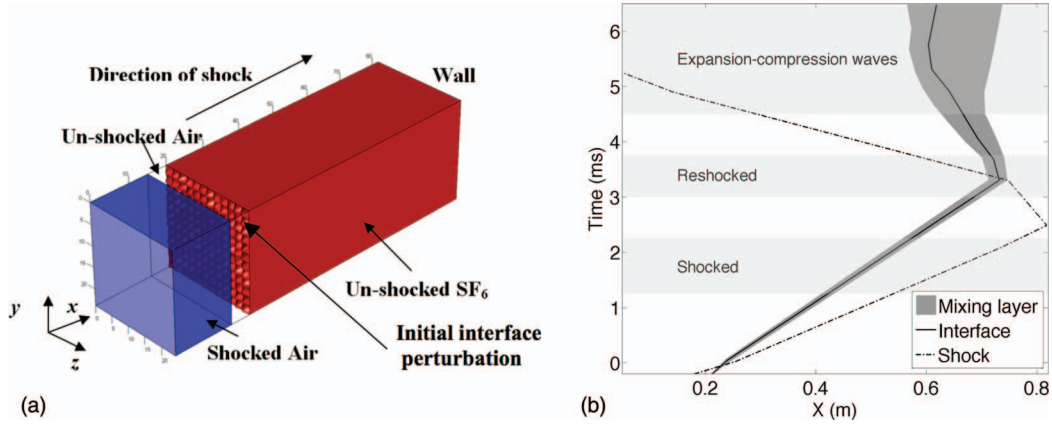
FIG. 1. Planar shocktube. (a) Flow configuration; (b) typical shock/interface evolution. Reprinted with permission from A. A. Gowardhan, J. R. Ristorcelli, and F. F. Grinstein, Phys. Fluids **23**, 071701 (2011). Copyright 2011 American Institute of Physics.

by the fluid physics involved: (1) large-scale entrainment, (2) stirring due to velocity gradient fluctuations, and (3) molecular diffusion. When convective time-scales are much smaller than those associated with molecular diffusion, we are primarily concerned with the numerical simulation of the first two convectively driven (interpenetration) mixing processes, which can be captured with sufficiently resolved implicit large eddy simulation (ILES).[23,24] ILES addresses the difficult issues posed by under-resolution, by relying on subgrid models provided implicitly by physics capturing numerics.

Here, we use an ILES simulation strategy that uses the Los Alamos National Laboratory (LANL) RAGE code[25] to investigate planar RMI. Issues of initial material interface characterization and modeling difficulties, and the effects of IC resolved spectral content on transitional and late-time turbulent mixing driven by planar RMI were investigated.[14] Three-dimensional (3D) simulations of shocked gas-curtain laboratory observations were also carried out[26] with the aim of characterizing the impact of 3D IC specifics on the gas-curtain dynamics and mixing. The cited work suggested that robust effective performances can be achieved with ILES in the RMI context despite uncertainty issues of IC characterization and modeling. The present work expands on our early investigation of the effects of initial interfacial morphology of the air-SF_6 interface in affecting planar RMI.[21]

RAGE solves the multi-material compressible conservation equations for mass density, momenta, total energy, and partial mass densities, using a 2nd-order Godunov scheme, adaptive mesh refinement (AMR), a variety of numerical options for gradient limiters and interface treatments. As used in the present work (with no interface treatments, and a van Leer limiter), RAGE models a Schmidt number $Sc \sim 1$ miscible material interface, and high-Re convection-driven flow with effective viscosity ν_{eff} determined by the small-scale cutoff.[14]

As in Ref. 5, integral measure analysis is based on transverse-plane and volume averaged quantities,

$$\langle f \rangle(x) = \int f(x, y, z) dy dz,$$

$$\bar{f} = \int \langle f \rangle dx, \tag{1}$$

$$Y_{SF_6} = \rho_{SF_6}/\rho, \quad \psi(x) = \langle Y_{SF_6} \rangle, \quad M(x) = 4\psi(x)[1 - \psi(x)], \quad \delta(t) = \int M(x) dx,$$

where ρ is the mass density, ρ_{SF_6} is the SF_6 partial mass-density, Y_{SF_6} is the SF_6 mass fraction, and $M(x)$, $\delta(t)$, are cross-stream averaged, and integrated mixedness, respectively. The volumetric average indicated by $\bar{f}$ denotes integration over the instantaneous mixing region, defined by a slab

TABLE I. Planar shock-tube simulations.

δ_o (cm)	0.5 (low-η_o)				5 (high-η_o)			
$(\lambda_{min}, \lambda_{max})$	$L(\frac{1}{24}, \frac{1}{6})$	$L(\frac{1}{12}, \frac{1}{4})$	$L(\frac{1}{6}, \frac{1}{3})$	$L(\frac{1}{4}, \frac{1}{2})$	$L(\frac{1}{24}, \frac{1}{6})$	$L(\frac{1}{12}, \frac{1}{4})$	$L(\frac{1}{6}, \frac{1}{3})$	$L(\frac{1}{4}, \frac{1}{2})$
κ_o (cm^{-1})	π	$\pi/2$	$\pi/4$	$\pi/6$	π	$\pi/2$	$\pi/4$	$\pi/6$
$\eta_o = \kappa_o \delta_o$	$\pi/2$	$\pi/4$	$\pi/8$	$\pi/12$	$10\pi/2$	$10\pi/4$	$10\pi/8$	$10\pi/12$
No. of modes	402	90	18	7	402	90	18	7

of volume V about the center of the mixing layer constrained in the x-direction by requiring $M(x)$ > 0.75. Analysis of turbulence characteristics is based on data deviations around transverse planes within the instantaneous mixing region, using,

$$\tilde{u}_i = \langle \rho u_i \rangle / \langle \rho \rangle , \quad u_i = \tilde{u}_i + u'_i, \quad \boldsymbol{\omega} = \nabla \times \mathbf{u},$$
$$r_{ij} = \langle \rho u'_i u'_j \rangle, \quad 2k = r_{ii}, \tag{2}$$
$$\rho = \langle \rho \rangle + \rho', \quad R = \langle \rho'^2 \rangle, \quad \upsilon = \langle \upsilon \rangle + \upsilon',$$

where $\boldsymbol{u}$ denotes the velocity field, and $\upsilon = 1/\rho$ is the specific volume; moreover, k is the local turbulent kinetic energy, ω^2 is the squared vorticity magnitude, R is the local mass-density variance, and we denote with K, Ω, and $\bar{R}$ their corresponding volumetric averages, respectively. Our notation here and in what follows assumes summation over repeated (Roman) indices, and we also use $()_{,i} \equiv \partial()/\partial x_i$.

A *sharp* interface (Fig. 2) morphology is defined in terms of $\chi(y,z)$ which denotes local material interface deviation about the mean. The local interface deformation is given by

$$\chi(y, z) = \Gamma \sum a_{nm} \sin(\kappa_n y + \phi_n) \sin(\kappa_m z + \varphi_m), \tag{3}$$

where $\kappa_n = 2\pi n/L$, $\kappa_m = 2\pi m/L$, $-1/2 < a_{nm} < 1/2$ are randomly selected coefficients, Γ is used to prescribe δ_o, $0 < \{\varphi_n, \varphi_m\} < 2\pi$ are phases randomly selected for each contributing mode, and the participating modes are constrained by the periodic boundary conditions through the requirement, $\lambda_{min} \leq L/[2\pi (n^2 + m^2)^{1/2}] \leq \lambda_{max}$ (actual number of contributing modes are quoted in Table I). The statistics of the initial interface, *rms* thickness, and *rms* slope, are then given by

$$\delta_o^2 = \langle \chi \chi \rangle, \quad \eta_o^2 = \kappa_o^2 \delta_o^2 = \langle \nabla \chi \nabla \chi \rangle, \quad \kappa_o^2 = \langle \nabla \chi \nabla \chi \rangle / \langle \chi \chi \rangle.$$

The meaning of these quantities is depicted in Fig. 2.

The quantity κ_o is used in the study of homogenous stochastic processes, where it is called the mean zero-crossing frequency.[27,38] The initial material interface value of κ_o is computed by checking for sign changes of the density fluctuation over lines within a transverse plane and ensemble averaging over the zero crossing occurrences (Fig. 3). In practice this is accomplished by computing λ_o – the mean zero crossing length (ZCL) – using the ideas depicted in the Figs. 2 and 3. The zero crossing wavenumber is computed using $\kappa_o = 2\pi/\lambda_o$, and the initial *rms* slope, η_o, follows from the formula.
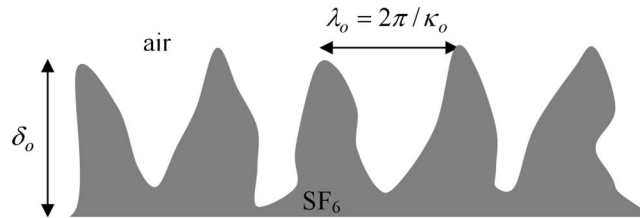

FIG. 2. Initial material interface characteristics. Reprinted with permission from A. A. Gowardhan, J. R. Ristorcelli, and F. F. Grinstein, Phys. Fluids **23**, 071701 (2011). Copyright 2011 American Institute of Physics.

FIG. 3. Zero-crossings of ρ'; L denotes the transverse dimension of the computational domain. Reprinted with permission from A. A. Gowardhan, J. R. Ristorcelli, and F. F. Grinstein, Phys. Fluids **23**, 071701 (2011). Copyright 2011 American Institute of Physics.
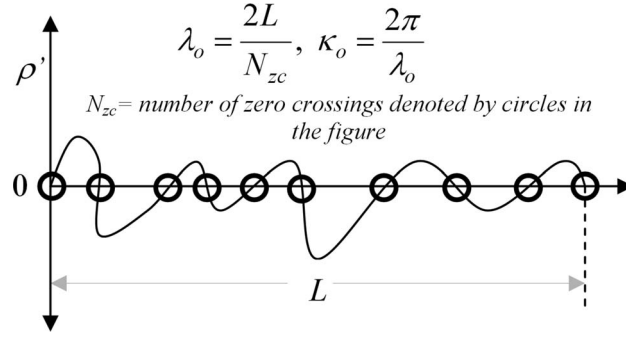
The same zero counting process is used at all subsequent time to compute $\lambda(t)$, $\kappa(t)$, and thus $\eta(t)$, the *rms* slope, as running variables. From the definitions it is straightforward to show a connection between the ZCL and the Taylor microscale of the density filed. For a homogeneous process on a plane the Taylor microscale is given by

$$\frac{1}{\lambda_T^2} = \frac{1}{2}\frac{\langle \nabla \chi \nabla \chi \rangle}{\langle \chi \chi \rangle},$$

and the ZCL and Taylor microscale are proportional.[38]

Various simulations based experiments were performed in terms of well-defined initial material interface perturbations and grid resolutions (using up to two levels of AMR refinement) were considered. The baseline resolution involved an $820 \times 240 \times 240$ grid ($\Delta_{\min} = 0.1$ cm); a much finely resolved $1640 \times 480 \times 480$ grid ($\Delta_{\min} = 0.05$ cm) was used for selected representative cases. The various cases are organized into two distinct categories having significantly different (low and high) initial *rms* slope η_o (Table I).

III. DEPENDENCE OF THE MIXING WIDTH ON η_o, THE *RMS* SLOPE OF THE INITIAL INTERFACE

We first focus on Fig. 4, which show the temporal evolution of the mixing layer width and its scalings for two different classes of L-H first shock simulations. We emphasize that the subject of our study the fluid dynamical response to the mixing layer being shocked and that our interest is on the early and intermediate times. Long-time asymptotic decay scalings are not our current interest.

As noted in our previous work,[14,21] inspection of the evolution of the mixing layer width $\delta(t)$ (Fig. 4(a)) for the low-η_o case shows growth rate trends are ordered in agreement with the predictions of the small perturbation linear impulse model of Richtmyer:[28] as the initial *rms* slope, η_o, is increased the layer grows faster and K is higher. The turbulent kinetic energy K produced by the interaction of the shock and the density interface is primarily in the direction of the shock, $\langle \rho u_1' u_1' \rangle \gg \langle \rho u_2' u_2' \rangle \approx \langle \rho u_3' u_3' \rangle$ leads to growth of the modes in the shock propagation direction and increased mixing layer widths with increasing η_o. The L-H low-η_o first shock cases generally have higher anisotropy than the L-H high-η_o cases (see below).

For large initial *rms* slope, the high-η_o cases, a trend that is exactly the opposite of the low-η_o case is seen: the *layer growth decreases* as η_o *increases*. The Richtmyer[28] scaling does not predict the ordering of the trends. For the high-η_o case there is a not only a much larger deposition of baroclinic vorticity but more importantly the vortex centers, whose distance is proportional to the ZCL, are closer to each other and they interact nonlinearly to produce more smaller scale flow features. The creation of new length scales, seen as an increase in the bandwidth of the flow (see below), is not seen in the low-η_o case. This gives rise to a very different scaling behavior as we explain in more detail in Sec. IV.
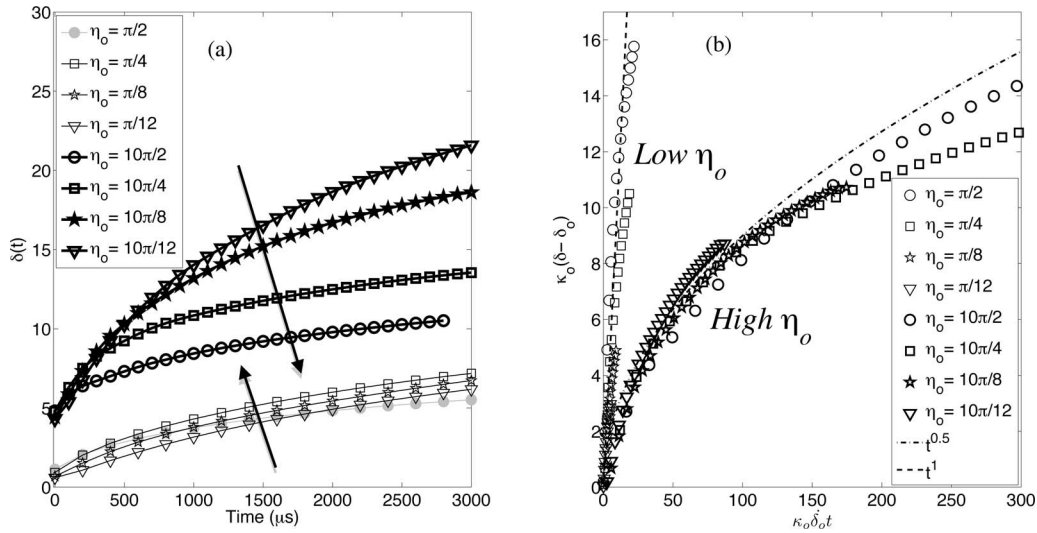
FIG. 4. Mixing width evolution for first shock low-η_o and high-η_o. (a) First-shocked only for low-η_o and high-η_o; (b) rescaled to collapse data. Arrows indicate the direction of increasing η_o. Reprinted with permission from A. A. Gowardhan, J. R. Ristorcelli, and F. F. Grinstein, Phys. Fluids **23**, 071701 (2011). Copyright 2011 American Institute of Physics.

Additional evidence for two different instability classes is seen by the scaling law collapse shown in Fig. 4(b). We follow Ref. 3 and plot the layer thickness $\kappa_o(\delta - \delta_o)$ versus time scaled with $\kappa_o\dot{\delta}_o$. Here, $\dot{\delta}_o$ is the initial mixing layer growth rate computed (using temporal central finite-differences) based on early-time simulation data *after* the shock has traversed the material interface. The less precise scalings for the faster-evolving high-η_o shocked mixing-layer widths after normalization with $\dot{\delta}_o$ reflect a historical rather than fundamental issue: our original study did not focus on early time aspects and, in hindsight, dumps in time (fixed dump interval $\sim$100 μs) were not frequent-enough to ensure uniformly accurate $\dot{\delta}_o$ for all cases compared.

The results for low-η_o and high-η_o in Fig. 4(b) tend to collapse into distinctly different scaling groups, $\delta \sim t$ or $\delta \sim t^{\frac{1}{2}}$, suggesting transition to a different class of flow physics above a threshold value $\eta_o \sim 1$ (for A and Ma specific to these simulations). These different trends demonstrate what we have called *the bipolar behavior of the RMI*.[21] In short, a flat interface and a very rough one (or equivalently a turbulent interface) react with very different instabilities. From the physical viewpoint one would like to understand the different physics; from an engineering model viewpoint one would like to be able to predict (model) these two classes of the RMI. The ($\delta \sim t^{\frac{1}{2}}$) scaling will be called the diffusive scaling, and ($\delta \sim t$) the ballistic scaling.

Figure 5 compares the evolution of a first shock L-H high-η_o mixing layer width with the corresponding low-η_o H-L reshocked cases. Before reshock, the trend of the dependence on η_o of the growth of the mixing layer is consistent with the conventional RMI, as say seen even in Richtmyer's original impulse theory;[28] the mixing layer grows faster as η_o is increased. After reshock, the mixing layer growth trends reverse: the mixing layer grows more slowly as η_o is increased. This is consistent with the first shock high-η_o regime behavior (Fig. 5(b)). The low-η_o interface at time of reshock has an *rms* slope, $\eta(t_{res})$, commensurate with the first shock of the high-η_o cases and exhibits the same high-η_o scaling behavior: the higher the *rms* slope at reshock, $\eta(t_{res})$, the lower the growth rate in direct contrast to the conventional small perturbation RMI trends.

A bulk *Re* built on the time-dependent mixing-layer width, $Re = \delta(t)\dot{\delta}(t)/\nu$, has been typically used to characterize the flow evolution of such simple flows, e.g., Ref. 29. In Fig. 6 we use $\delta(t)\dot{\delta}(t)$ to indicate the relative behaviors of the mixing layer growth trends between L-H first-shocked high-η_o and H-L reshocked low-η_o cases. Evidence for the fluid physics responsible for these similarities between two fairly distinct classes of flows is discussed from the point of view of statistical moments of the flow in Secs. IV and V.
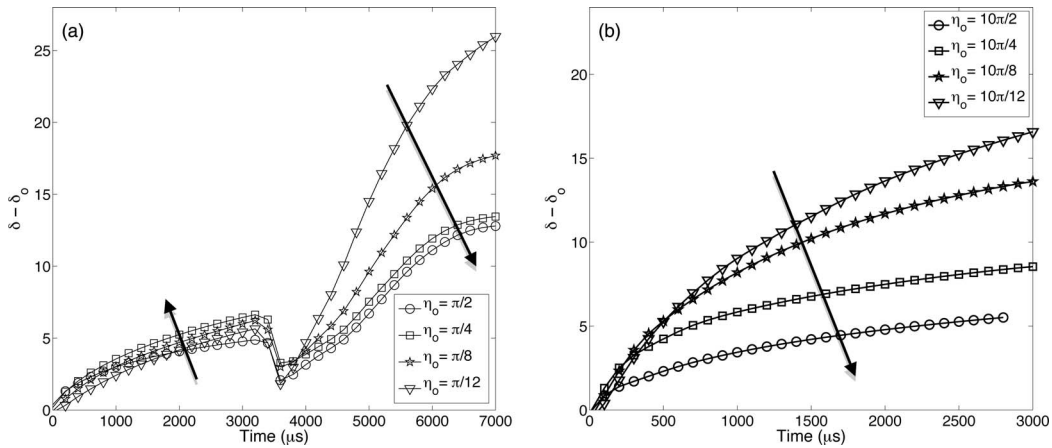
FIG. 5. Mixing width growth. (a) Low-η_o first-shocked/reshocked; (b) high-η_o first-shocked only. Arrows indicate the direction of increasing η_o. ICs at $t = 0$ are characterized by the single parameter η_o.

IV. COMPARISON OF THE STATISTICS OF THE TWO FLOW CLASSES

Our observations above regarding the effects of the initial interfacial morphology indicate that, for the high-η_o L-H case, the accelerated interface develops into a nonlinear regime with very different scaling behaviors than the RMI scaling seen in the low-η_o case, namely, the $\delta \sim t^{\frac{1}{2}}$ "diffusive" scaling versus the $\delta \sim t$ "ballistic" scaling, respectively. In this section, we study and compare the low-η_o first-shocked L-H and the H-L reshocked cases with the high-η_o L-H first-shocked case. In preview, we observe similar ordering of trends of the reshock cases with the high-η_o first-shock case. As it turns out, the interface *rms* slope $\eta(t_{res})$ at reshock time is commensurate with the first-shocked high-η_o case and exhibits the same scaling law behavior once above some threshold value, i.e., the higher the initial *rms* slope at shock, the lower the growth rate. Using metrics from equilibrium turbulence vocabulary, we discuss and connect these two diverse behaviors through description of the fluid-physics.
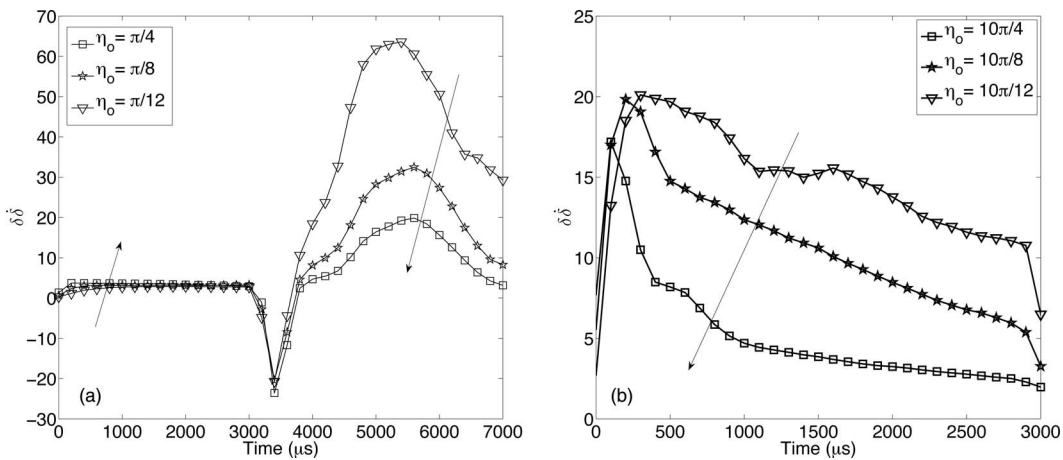

FIG. 6. The evolution of a bulk *Re*. (a) Low-η_o first-shocked/reshocked; (b) high-η_o first-shocked only. Units are m^2/s. Note that at $t \sim 5000$ μs on (a) the second (reflected compression wave) reshock occurs increasing the energy of the layer. Arrows indicate the direction of increasing η_o.
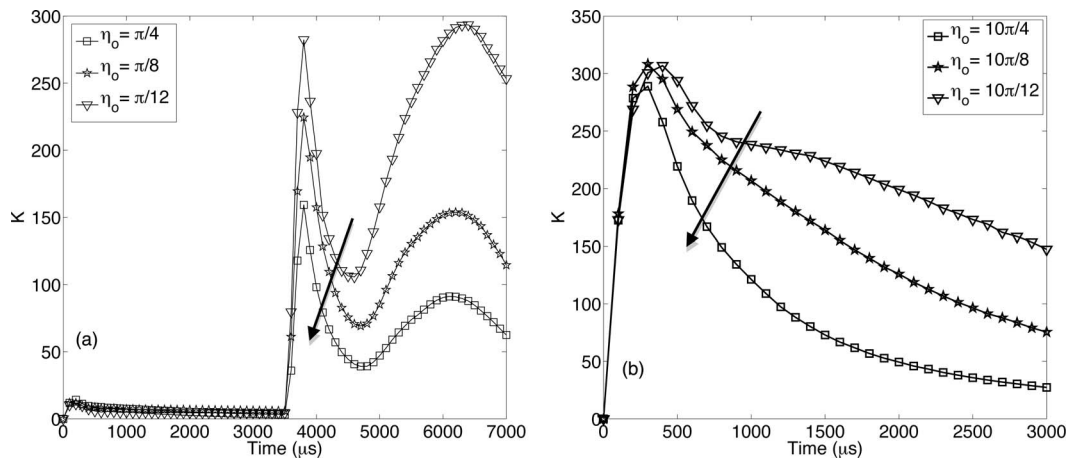
FIG. 7. Turbulent kinetic energy. (a) Low-η_o first-shocked/reshocked; (b) high-η_o first-shocked only. The arrows indicate the direction of increasing η_o. Not shown are the arrows for the pre-reshock low-η_o case. Note that at $t \sim 5000\ \mu$s on the left hand side the second (reflected compression wave) reshock occurs increasing the energy of the layer.

A. Energy

Figure 7 show the turbulent kinetic energy K as a function of time. The first-shocked L-H low-η_o has very little energy compared to either the H-L reshocked case or the first-shocked high η_o case, in fact, they differ *by orders of magnitude*. In the low-η_o first-shocked/reshocked cases, at $t \sim 5000\ \mu$s the reflected shock from the back wall increases the energy substantially; the period of the flow for $t > 5000\ \mu$s is not of direct interest to our study of the behavior of the two instabilities. Our focus is on the evolution of flow quantities immediately after reshock and before occurrence of the reflected compression-wave reshock, $t < 5000\ \mu$s. We note the ordering of the K curves, once a threshold value has been passed, with increases in the *rms* slope at time of shock: the higher the η_o or $\eta(t_{\rm res})$ the lower the energy, K. This is opposite to the H-L low-η_o case for which K increases with increasing η_o (see also Ref. 21). We reiterate our interest in studying the nature of the instabilities and not the asymptotic temporal power-law scalings of the decay period.

B. Enstrophy

Similar statements can be made for the enstrophy. To leading order the enstrophy Ω scales the dissipation ε , as, $\varepsilon = \nu \overline{\langle \omega^2 \rangle} = \nu \Omega$. Figure 8 shows the turbulent enstrophy as a function of time. The L-H first-shocked low-η_o has very little enstrophy compared to either the H-L reshocked case at and the L-H high-η_o shock case; again they differ by orders of magnitude. In the reshocked cases, at around $t \sim 5000\ \mu$s (depending on case) the reflected shock from the back wall increases the enstrophy substantially. Note again the ordering of the enstrophy in the high-η_o and high with η_o or $\eta(t_{\rm res})$ cases: the higher the *rms* slope the higher the enstrophy. Singularly compelling, and consistent with the notion of a turbulent flow with nonlinear cascade is the fact that both cases with the highest early-time enstrophy have the least amount of enstrophy at some intermediate later time. The characteristic time scale of turbulent decay which scales as $\sim \Omega/K$ is very different as function of η_o or with η_o or $\eta(t_{\rm res})$ and this manifests itself in a more rapid decay of the enstrophy for the highest η_o (Fig. 8(b)). We make a point here about modeling – which we return to below: the assumption made in most turbulence models is that the production of enstrophy is proportional to the production of turbulent kinetic energy and, we speculate – given the present results, that this may not be useful for this non-equilibrium flow near the enstrophy deposition stage.
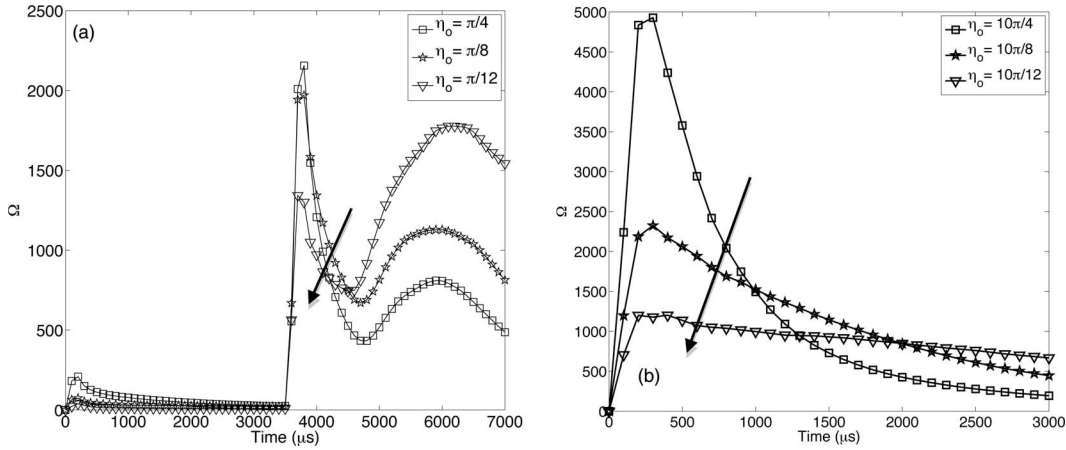
FIG. 8. Enstrophy. (a) Low-η_o first-shocked/reshocked; (b) high-η_o first-shocked only. The enstrophy increase at t $\sim$ 5000 μs on (a) reflects occurrence of the reflected compression wave reshock.

C. Anisotropy

We now investigate the anisotropy of the fluctuating velocity fields using the anisotropy tensor b_{ij},[34] defined in terms of the Reynolds stress r_{ij},

$$b_{ij} = r_{ij}/r_{kk} - \tfrac{1}{3}\delta_{ij}. \tag{4}$$

The tensor b_{ij} is bounded, i.e., $-1/3 \leq b_{ij} \leq 2/3$, with $b_{\alpha\alpha} = -1/3$ and $b_{\alpha\alpha} = +2/3$, corresponding to having either no turbulent kinetic energy or all of the energy, respectively, in the (α,α) component of b_{ij}, and $b_{\alpha\alpha} = 0$ for all α corresponds to the isotropic turbulence limit. As the tensor is trace-free, $b_{ii} = 0$, and because it is statistically symmetric, $b_{22} = b_{33}$, and we use $b_{11} = r_{11}/2k - 1/3$; $\overline{\langle b_{11}\rangle}$ is plotted in Fig. 9. In general, the high-η_o case and the low-η_o reshock case have much lower anisotropy as a consequence of the nonlinear interactions that distribute the energy amongst the different components. At the end of the low-η_o simulation (before reshock) one has $\overline{\langle b_{11}\rangle} \sim 0.28$ which corresponds to three-times as much energy in the axial direction as compared to either of the transverse directions. At the end of the low-η_o simulation after reshock, and at the end of the high-η_o case, the anisotropy is much lower, $\overline{\langle b_{11}\rangle} \sim 0.1$, corresponding to about 30% more energy in the axial component as compared to either of the transverse components.
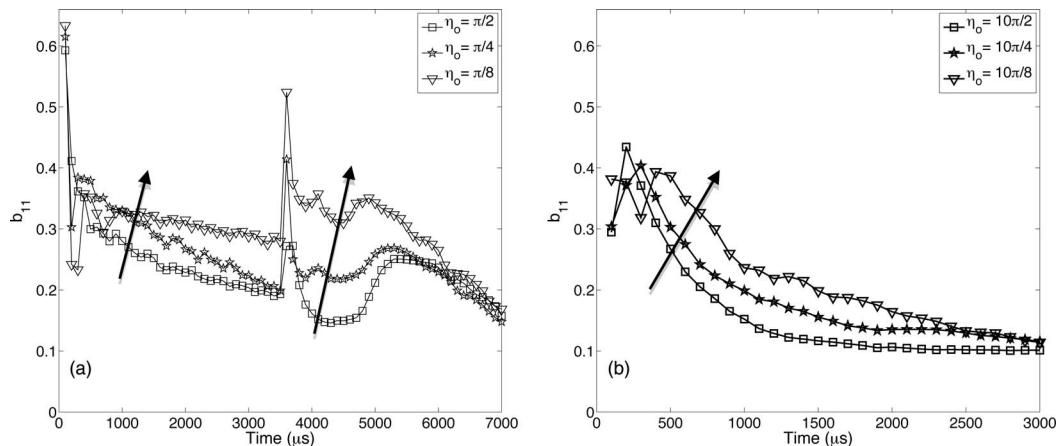

FIG. 9. Anisotropy evolution. (a) Low-η_o first-shocked/reshocked; (b) high-η_o first-shocked only.

The trajectory towards isotropy is due to nonlinear effects manifesting through the pressure-strain correlation in the Reynolds stress equations.[30] Unlike the kinetic energy and material mixing the anisotropy decreases with increases in η_o whether one is in the high-η_o or the low-η_o class of the RMI. Thus, the high-η_o or low-η_o case behaves similarly regarding anisotropy unlike most other statistics that exhibit the bipolar behavior.

D. A spectral bandwidth proxy

Measures of transition to turbulence are inherently as multi-valued as the definition one chooses to uses to define turbulence. At the very simplest end, transition to turbulence is seen as rapid increase in population of motions with smaller length scales, which for equilibrium turbulence can lead to an inertial subrange in the turbulent kinetic energy spectra (see, e.g., Ref. 30 and references therein). The spectral bandwidth of equilibrium turbulence is scaled by a power of the turbulent Re, usually taken as a ratio of integral-to-Kolmogorov length scales, or ratio of integral-scale (ℓ) to Taylor-microscale (λ), for example,

$$\lambda/\ell \sim 1/\sqrt{\mathrm{Re}_\ell} \sim 1/\mathrm{Re}_\lambda, \tag{5}$$

as given in Ref. 30, with $\lambda^2 = \langle u^2 \rangle / \langle (u_{1,1})^2 \rangle$, and $\ell = K^{3/2}/\varepsilon$.

In our preliminary exploration oriented context, we use the thickness of the layer, $\delta(t)$ as an approximation for the integral scale, and the mass-density Taylor microscale $\lambda(t)$ – related to the spatial zero crossing frequency through $\lambda(t) = 2\pi/\kappa(t)$ – as proxy for the scales at the higher end of the inertial range. Thus $\eta(t) = \kappa(t)\delta(t)$ is a qualitative measure of the *spectral bandwidth*. The symbol η thus plays two roles: as η_o it describes the initial interface and as $\eta(t)$ it is a running *spectral bandwidth* variable.

Figure 10 shows that the *rms* slope of the interface $\eta(t)$ increases with time. As the flow becomes nonlinear (high-η_o), one observes increased production of small-scales motions at early times as indicated by higher $\eta(t)$ and longer self-similar ranges in the spectra (see Fig. 10(b) and Ref. 14). The late time saturation of $\eta(t)$ for the highest η_o in Fig. 10(a) indicates faster disappearance of small scales by extraction via the cascade mechanism (see also discussion of Fig. 12 below) associated with the higher Reynolds number flow. As in Ref. 14, the *q-shelled* spectra are obtained by averaging 2D $E_R(q)$ evaluated at cross-stream planes within the mixing slab region defined above. This is consistent with what was seen for the enstrophy: the higher the early time enstrophy the sooner the flow produces more scales through nonlinear processes as seen in an increase in our spectral bandwidth measure in Figs. 10 and 11 and the faster the enstrophy and energy decays. This is
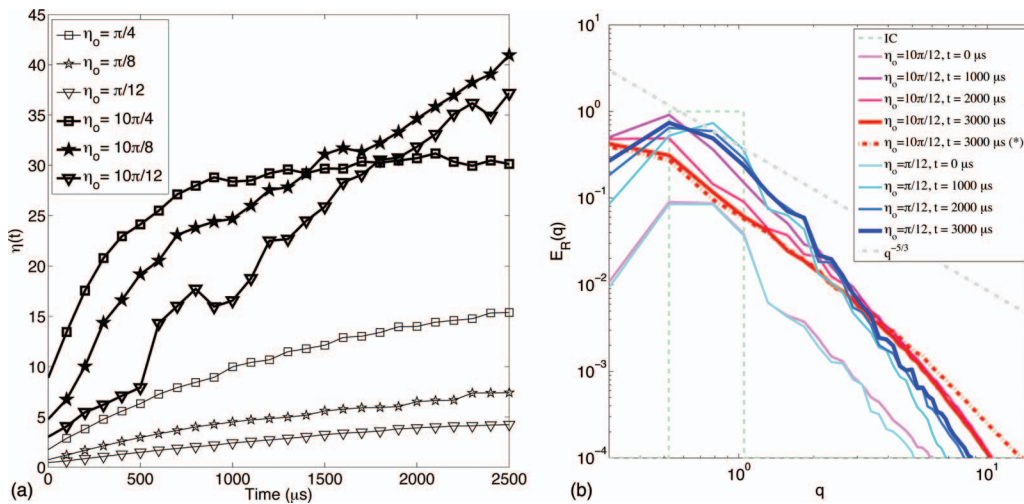

FIG. 10. (a) and (b) Spectral bandwidth and energy spectra evolution: first-shocked cases only; $E_R(q)$ spectra at representative times are shown in (b), where (*) denotes finer resolution results (see also Fig. 11).
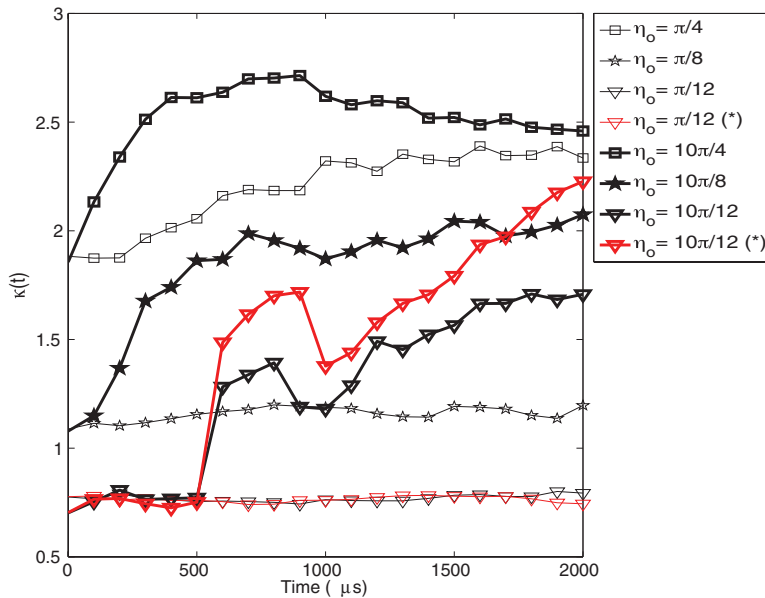
FIG. 11. Taylor mass-density microscale wavenumber: evolution of wavenumber $\kappa(t)$ after first-shocked low and high η_o cases. The cases with (*) denote finer (doubled) resolution results; in the worst-case resolution scenarios, i.e., shortest IC wavelength sets ($\eta_o = \pi/4$ and $\eta_o = 10\pi/4$), 20–60 cells/wavelength were involved on the coarsest grid (and 40–120 on the finest).

consistent with standard notions regarding decaying turbulence, that, e.g., the higher the enstrophy, the sooner the flow goes into a decay mode accompanied by a decrease of the spectral bandwidth measure (Fig. 10), and the more rapid decrease in energy and enstrophy—Figs. 8 and 9. This is a highly non-equilibrium flow and the higher η_o in the high-η_o cases, the larger the cascade rate, the more rapidly the decay process of both K and Ω occurs.

It is useful to separately investigate the zero crossing wavenumber portion of $\eta(t)$. The evolution of $\kappa(t)$ of the mass-density field is shown in Fig. 11 for the high-η_o and low-η_o L-H first-shocked cases *which all start with the same initial wavenumber*. For the high-η_o cases, one sees a sudden increase in the $\kappa(t)$ corresponding the creation of additional smaller scales of the motion. It is interesting to note that at the time the $\kappa(t)$ of the three high-η_o simulations take a sudden increase is also where the bulk *Re* suddenly starts to decay, see Fig. 6. This is consistent with the notion that the extraction of energy from the large scales by a nonlinear cascade to smaller scales increases with the appearance of additional scales, a feature only possible through a nonlinear process. The appearance of the nonlinear cascade is the primary physical process that distinguishes the high-η_o from the low-η_o case—in which the Taylor microscale stays reasonably constant (and fairly grid independent) and there is no cascade (Figs. 10(b) and 11). The finer resolution results in Fig. 11 also show higher Taylor density microscale for high-η_o (and somewhat longer inertial range in Fig. 10(b))—consistent with higher *Re*.[14]

Our low-η_o L-H first-shocked results are consistent (in not showing transition before reshock) not only with our own previously reported ($A > 0$, low-η_o) results *before reshock*[14] but also with those of Pullin *et al.*[10] using a classical LES strategy, different numerics, and similar resolution for the same planar RMI problem, and (as in Ref. 10) predict mixing width growth rates in agreement with the laboratory experiments.[4] The fact that both cited simulations[10,14] show *non-transition* before reshock suggests an effective resolution-dependent *Re* below the mixing-transition *Re* threshold.[32] The RMI ILES work by Cohen *et al.*,[8] also involving $A = 0.67 > 0$ and $Ma = 1.5$, addressed first-shocked mixing only for the planar RMI experiments in Ref. 4 using the finest reported grid resolutions: 50–200 cells per characteristic wavelength of the dominant initial material interface perturbation (the so-called *egg crate* mode). In contrast, 10–20 cells per wavelength were used in Refs. 10 and 14, and at least 20–40 here (and in Ref. 21). Cohen *et al.*[8] show evidence of both,
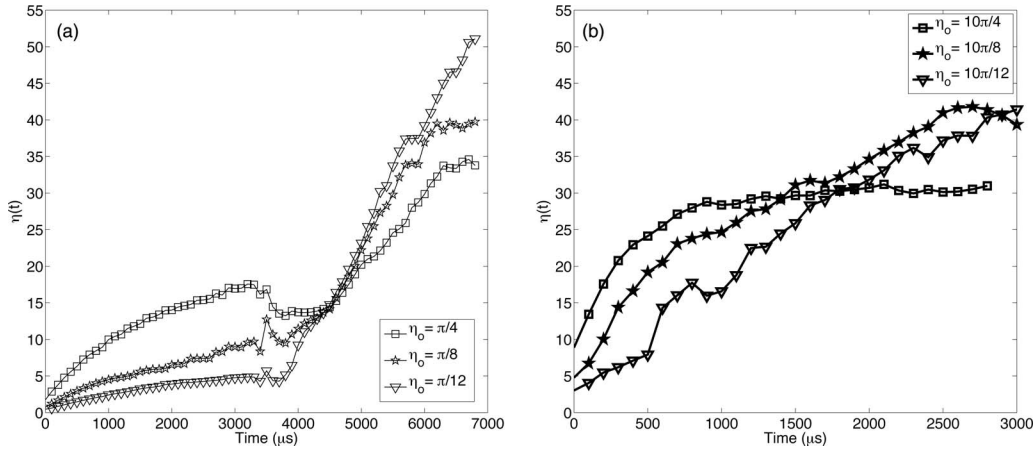
FIG. 12. "Spectral bandwidth" measure $\eta(t)$. (a) Low-η_o first-shocked/reshocked; (b) high-η_o first-shocked only.

laminar and transitional behavior on first-shock for a given A and Ma, depending on grid resolution and associated effective Re.[14]

We now compare the low-η_o L-H first-shocked and the H-L reshocked case with the high-η_o L-H first-shocked only case. Late-time $\eta(t)$ in Fig. 12(b) gives the initial rms slope at reshock (for $t \sim 3000$–$4000 \ \mu s$); when $\eta(t) > \pi/2$—high enough for transition to nonlinearity to become possible. Figure 12(a) shows the evolution of $\eta(t)$ after the mixing layer is reshocked. The fact that $\eta(t)$ increases with time for all cases suggests that spectral bandwidth is increasing—which can also be understood as an increase in turbulent Re.[22,30] For the low-η_o cases, the increase in $\eta(t) = \kappa(t)\delta(t)$ is due to the increase $\delta(t)$. In the section on mixing below it is shown that $\kappa(t)$ becomes relatively constant as no new scales are created and the small scales are simply decaying by a flow with very little enstrophy. As noted earlier in connection with Fig. 10(a), the late time saturation of $\eta(t)$ for the highest η_o in Fig. 12(b), indicates faster disappearance of small scales by extraction via the cascade mechanism. Due to mode coupling, there is a much larger (and faster) increase in spectral bandwidth for the high-η_o cases which are then followed by a faster decay due to the stronger mode coupling. This is consistent with heuristic notions of the presence of a nonlinear cascade characteristic of turbulent flow. Our observations suggest that sudden increases in $\eta(t)$ and $\kappa(t)$ can be consistently used as basis for metrics to indicate a transition to a different class of flow physics.

E. Turbulent eddy viscosity

The same ideas can be discussed using the turbulent eddy viscosity, $\nu_t = K^{1/2}\delta(t)$, a cornerstone modeling assumption in simple turbulence closure. Note that if $K^{1/2} \ \delta(t)$ is normalized by a fluid viscosity it can be interpreted as a bulk turbulent Re; our interest is in the un-normalized quantity as a measure that a standard moment closure might use to compute turbulent transport. In Fig. 13(b) we see that the high enstrophy case – what we have called the more turbulent and which (up to a point in which the decay sets in strongly) has a higher bandwidth – has a lower turbulent viscosity as the very high level of enstrophy has dissipated the energy much more rapidly than in the lower η_o case of the high-η_o group. After the passage of the shock the turbulence is a decaying turbulence in which the flow with the highest level of enstrophy after shock deposition (and enstrophy creation) will decay the fastest by cascade.

F. Summary of statistical analysis

Our analysis on the effects of initial interfacial morphology indicates that for high $\eta(t_{res})$ or η_o, the RMI develops directly into a nonlinear regime and becomes a flow producing more and more small scales through nonlinear model coupling processes characteristic of vorticity amplification of a
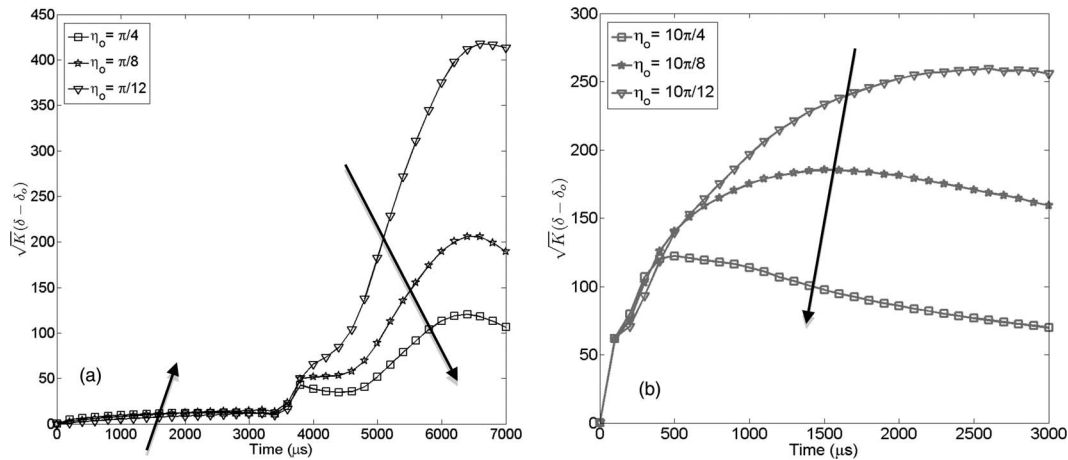
FIG. 13. Turbulent eddy viscosity: $\nu_t = K^{1/2}\delta(t)$. (a) Low-η_o first-shocked/reshocked; (b) high-η_o first-shocked only. Note that at $t \sim 5000\ \mu$s on the left plot a second reshock is occurring and that increases the energy a second time. Units are m^2/s.

cascade. In addition, the transition of the highest η_o reshock case to a decaying turbulence (beginning of the decrease of the spectral bandwidth measure) is also seen in the high η_o suggesting a remarkable consistency in the flow physics as captured by the $\eta(t) = \kappa(t)\delta(t)$ measure. A self-consistent picture emerges not only between low and high-η_o, $\eta(t_{res})$, cases but also within the high-η_o cases: one sees that the flow with the most enstrophy – ostensibly the initially most turbulent by the conventional notions – ends up being the least turbulent (having the least enstrophy) due to the increased cascade rate and dissipation and in all the plots the most initially turbulent flow decays fastest and becomes the least turbulent (using any of the above measures) by the end of the simulation. This picture supports our finding that RMI turbulence can be achieved on the first shock if the interface has large enough *rms* slope.

Within each of the two classes of ICs (high η_o *or* $\eta(t_{res})$, and low-η_o) the response of the rate of growth of the RMI mixing layer width to the increase of η_o is opposite. For the low-η_o class of interfaces, the growth of the mixing layer appears driven by vorticity deposition with little mode coupling and the evolution of the RMI layer scales as $\delta \sim t$ and trends follow Richtmyer's impulsive scaling.[28] Increasing η_o in the low-η_o classes increases the deposition of baroclinic vorticity on the initial material interface and leads to higher layer growth. For the high-η_o and $\eta(t_{res})$ class of interfaces, the growth of the mixing layer appears driven by vorticity deposition and importantly a large amount of additional vorticity is created through mode coupling and the evolution of the RMI layer scales as $\delta \sim t^{\frac{1}{2}}$, and trends do not follow the impulse scaling. It is pertinent to recall that – in three-dimensional flows – vorticity (or enstrophy) is not a conserved invariant and is created by nonlinear processes. In contrast, increasing η_o in the high-η_o group also increases the deposition of baroclinic vorticity, but this leads to a reduced mixing width growth rate $\delta \sim t^{\frac{1}{2}}$, associated with the production of new small scales by nonlinear mode coupling that are additionally dissipative. The two RMI flow types are summarized with the following heuristic:

$$
\begin{aligned}
&low-\eta_o, \quad \delta \sim t: \quad as\ \eta_o \uparrow \quad \Omega \uparrow \quad b_{11} \downarrow \quad K \uparrow \quad \delta \uparrow, \\
&high-\eta_o, \quad \delta \sim t^{1/2}: \quad as\ \eta_o \uparrow \quad \Omega \uparrow \quad b_{11} \downarrow \quad K \downarrow \quad \delta \downarrow.
\end{aligned}
\tag{6}
$$

The low-η_o case is consistent with the idea of little mode coupling and a linear growth $\delta \sim t$ whose trends are consistently ordered with the impulse theory of Richtmyer. This is the case of a first shock on a relatively smooth interface. The high-η_o case is consistent with the idea of a nonlinearly mode-coupled flow with diffusive growth law $\delta \sim t^{\frac{1}{2}}$ whose trends – after the spectral broadening phase – are consistent with what is known of the decay of isotropic turbulence (see below). The low-η_o reshock cases which have high $\eta(t_{res})$ follow all the trends of the high-η_o cases. We have not

been able to verify the $\delta \sim t^{\frac{1}{2}}$ scaling for the reshock case as the occurrence of the second reshock is too soon for a robust scaling to appear.

The remarkable fact is that the increase of enstrophy that accompanies the increase in η_o in both linear ballistic and nonlinear diffusive cases leads to two very different fluid dynamical responses: in the low-η_o case the kinetic energy *increases* due to higher deposition of energy while in the high-η_o or $\eta(t_{res})$ "nonlinear" case there is a production of new smaller scale motions and a *reduction* in kinetic energy as would accompany a cascade of energy to small scales. While the configuration corresponds to the Richtmyer-Meshkov geometry it appears that there are two very different instabilities.

V. ANALYSIS OF MATERIAL MIXING

In this section we give observations on the mixing process seen in the simulations. First we present images to illustrate what the data suggest. We show how a consistent picture emerges when looking at analysis based on the ZCL, the probability density function (PDF) of Y_{SF_6}—Fig. 15, and second order moments. We provide some statistics of the material field used in second order moment closures for variable density turbulence. The statistical analysis is done as noted earlier in the instantaneous mixing region, defined by the slab of volume V about the center of the mixing layer constrained in the x-direction by requiring $M(x) > 0.75$. The slab involves a cross section of the shock tube ($Ly \times Lz$). PDFs are computed based on individual Y_{SF_6} values within this slab. For each time, the slab contains 120 data points in the y and z directions for the coarse resolution and 240 cells for the fine resolution case. The number of cells in the shock direction varies with time as the region is constrained by $M(x) > 0.75$.

In Fig. 14 the instantaneous mass fraction fields for the nine cases are shown. The mass fraction of SF$_6$ at selected times, $t = 3000$ μs after the first shock (or $t = 3000$ μs after reshock). In columns 1, 2, and 3, first-shocked L-H low-η_o case, reshocked H-L low-η_o case, and first-shocked
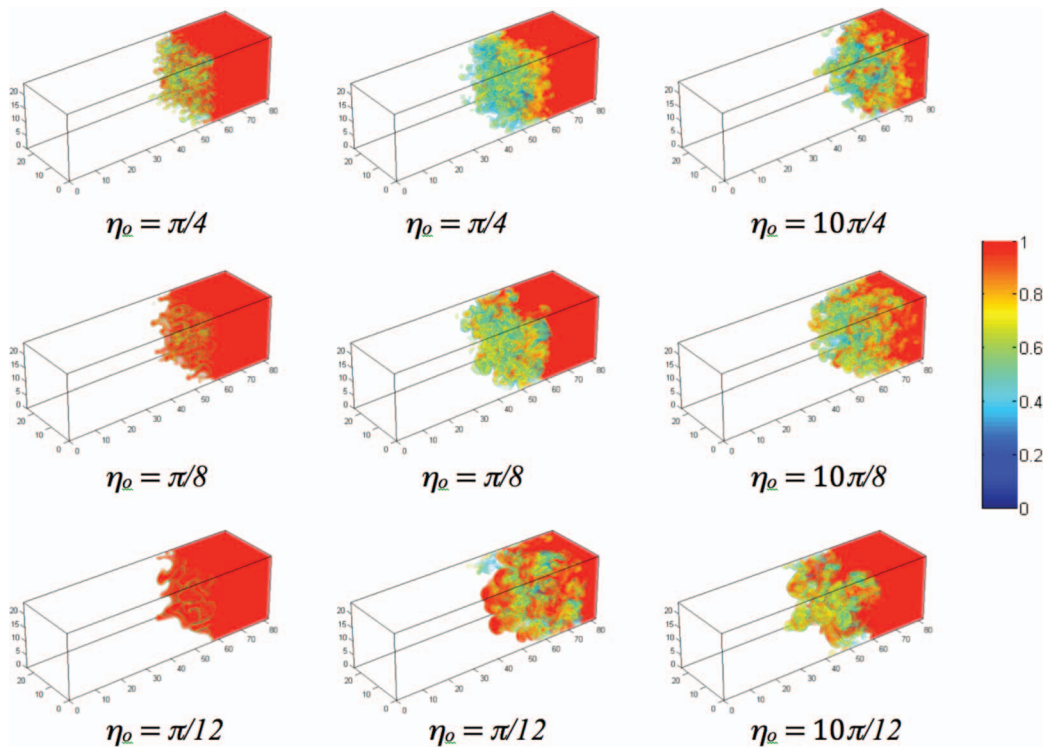

FIG. 14. Mixing visualizations. Column 1: first-shocked low-η_o case. Column 2: low-η_o after being first-shocked/reshocked. Column 3: first-shocked high-η_o case. Images taken at $t = 3000$ μs after first-shock (columns 1 and 3) or $t = 3000$ μs after reshock (column 2).
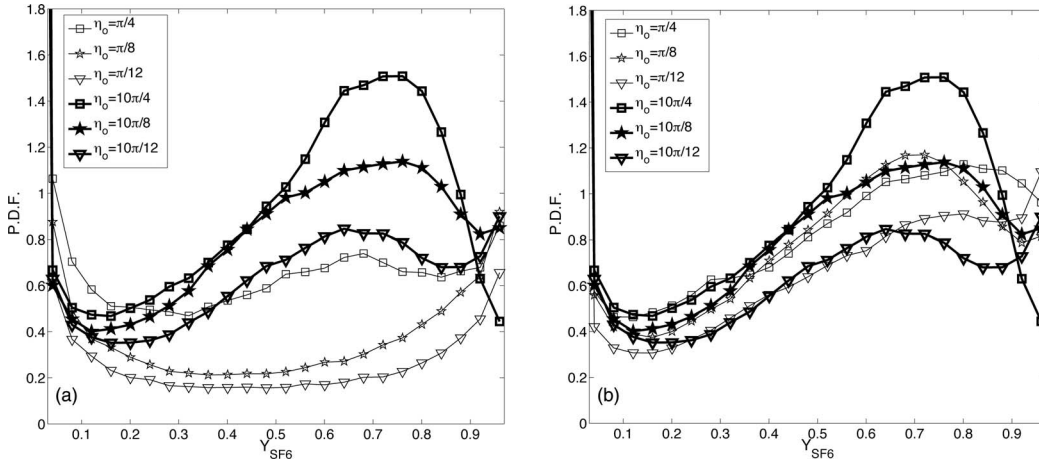
FIG. 15. PDFs of Y_{SF_6} for: (a) high-η_o and low-η_o first-shocked; (b) first-shocked high-η_o and first-shocked/reshocked low-η_o. Plots for same times as in Fig. 14, and PDFs at $t = 3000$ μs after first-shocked-only or $t = 3000$ μs after reshock.

L-H high-η_o case, respectively, are shown. The point here is that there is much less mixing for the low-η_o first-shocked case as compared to the other two cases; this is consistent with the much lower energy and enstrophy and initial behavior of the ZCL as indicated above. The primary point is that the similarity between hydro-dynamical statistics of the first-shocked L-H low-η_o case and the H-L reshocked low-η_o case and the first-shocked L-H high-η_o case seen above is consistent with what is observed in the material fields.

Many of the observations we have made regarding turbulence level are substantiated by the PDFs for the material field. In general, the higher the η_o, the higher the turbulence level, and the more mixed the fluid as seen by a PDF that becomes more unimodal. We see an approximately bimodal distribution for the low mix and low-η_o first-shocked-only cases in Fig. 15(a) indicating regions of pure fluid in the sampling region. The PDF has maxima associated with the two pure fluids indicating that important levels of unmixed fluid remain. The high-η_o cases (and the one intermediate case) have a more unimodal distribution with maxima in the mixed fluid region of the PDF. This is consistent with the very different levels of turbulence and more rapid mixing with the first shock L-H high-η_o cases. Figure 15(b) compares the L-H high-η_o first-shocked cases and the low-η_o L-H first and H-L reshock cases and shows similar unimodal behavior characteristic of faster mixing processes. Thus the high-mix PDFs support our interpretations regarding the bipolar behavior of the RMI and the magnitude of the turbulence generated.

A. The zero crossing wavenumber

One can also study the mixing process using the ZCL (or Taylor microscale) of the density field, λ, which assigns a characteristic length scale to the material field. From the viewpoint of the theory of homogeneous stochastic processes, λ is the mean distance between zero crossings of a realization of a zero mean process and this is how we calculate it once the flow has evolved. From the correlation function viewpoint, λ is related to the radius of curvature at the origin of the two-point spatial correlation and is thus mathematically equivalent to the Taylor microscale of homogeneous turbulence. As noted above, we use the interpretation of λ as a mean ZCL to compute it and interpret it as a statistical measure of the material "blob" size. And since we are not in fully developed homogenous equilibrium turbulence we shall use the term ZCL rather than Taylor microscale in our discussion to avoid any associations with a problem that does not resemble the RMI. The wavenumber $\kappa(t)$ associated with the ZCL $\lambda(t)$ through $\lambda(t) = 2\pi/\kappa(t)$ was weighted by the layer thickness $\delta(t)$, in $\eta(t) = \kappa(t)\delta(t)$—used above as a qualitative measure of spectral bandwidth. The behavior of $\lambda(t)$ (or $\kappa(t)$) supports a consistent viewpoint of our interpretation of the two classes of instabilities.
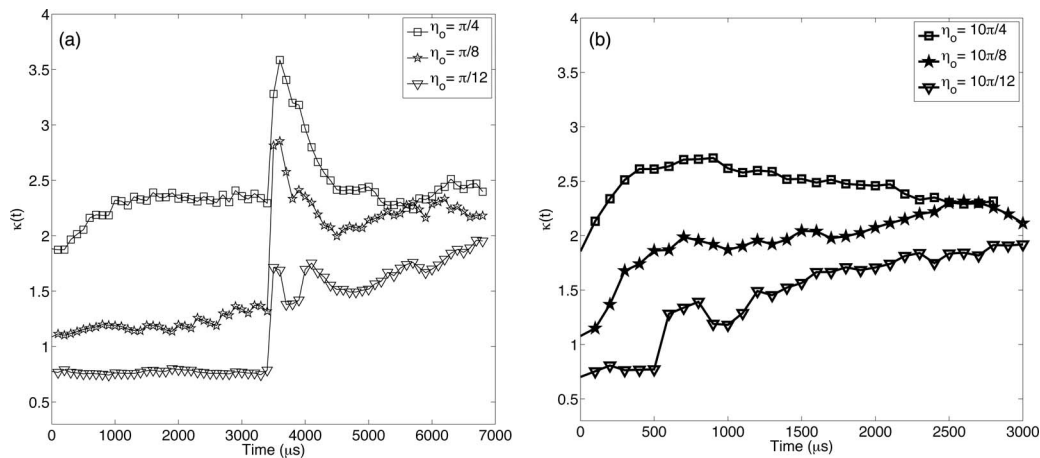
FIG. 16. Density Taylor microscale wavenumber. (a) Low-η_o first-shocked/reshocked; (b) high-η_o first-shocked-only (see also Fig. 11).

The evolution of the ZCL wavenumber $\kappa(t)$ of the density field is shown in Fig. 16(a) for the low-η_o first-shocked/reshocked case and in Fig. 16(b) for L-H high-η_o first-shocked only cases (see also Fig. 11). For the latter high-η_o cases, one sees at some point a sudden increase in the $\kappa(t)$ corresponding to a decrease in the typical statistical blob size of the density field due to the creation of additional smaller scales of the motion. It is interesting to note that the time when the $\kappa(t)$ of the three high-η_o simulations takes a sudden increase is also where the bulk Re starts to decay, see Fig. 6. This is consistent with the notion that the transfer of energy by the nonlinear cascade to smaller scales increases with the appearance of additional scales, a feature only possible through a nonlinear process. As noted before in connection with Fig. 11, the appearance of the nonlinear cascade and the creation of more smaller scales is the primary physical process that distinguishes the low-η_o first-shocked-only cases – in which the ZCL stays reasonably constant – from the H-L reshocked flow and the L-H high-η_o first-shocked-only case.

B. Second order moments of the material field

We present additional material field statistics in order to make the presentation more comprehensive, point out some very interesting findings, and provide insights into material mixing relevant to moment closure models. The key finding here is that the high-η_o/low-η_o bipolar behavior observed in the hydrodynamic field is also seen in the material field at early time but not at later time for the low-η_o case. This is an important finding as most turbulence models slave the material mixing to the turbulence field and the behavior of the two fields does not track each other for the low-η_o case after an intermediate period of time. The reason for the disparity is that unlike the enstrophy field which is generated by the nonlinear cascade mechanism *and* baroclinicity, the mixing rate field has only the cascade mechanism as a production term.

Figures 17 and 18 give the second order moments of the material field, the averaged mass-density/specific-volume covariance, $b_{avg} = -\overline{\langle \rho' \upsilon' \rangle}$ and the mean mass-density variance $\overline{\langle \rho'^2 \rangle}$. The quantity b is of interest in the context of variable-density moment closure strategies,[30,41] where $b\langle P_{,i} \rangle$ appears as a production term in the transport equation for the turbulent mass flux, $\langle \rho' u'_j \rangle$. The turbulent mass flux in the presence of a pressure gradient is the primary source of kinetic energy of the turbulence. At early time, the moments are ordered by the expected low-η_o scaling and are similar to the low-η_o trends of the hydrodynamic field. At some intermediate time, before reshock, the order of the trends with η_o changes. At early time, the higher the η_o the larger the amount of both second order moments produced and also the larger the amount of the production of the mixing rate by the stirring $\langle \rho'_{,i} S_{ij} \rho'_{,j} \rangle$, where $S_{ij} = u'_{i,j}$ is the fluctuating strain rate.[22,42] Thus, there is more rapid decay of both second order moments with higher η_o. At some point in time the lower η_o cases
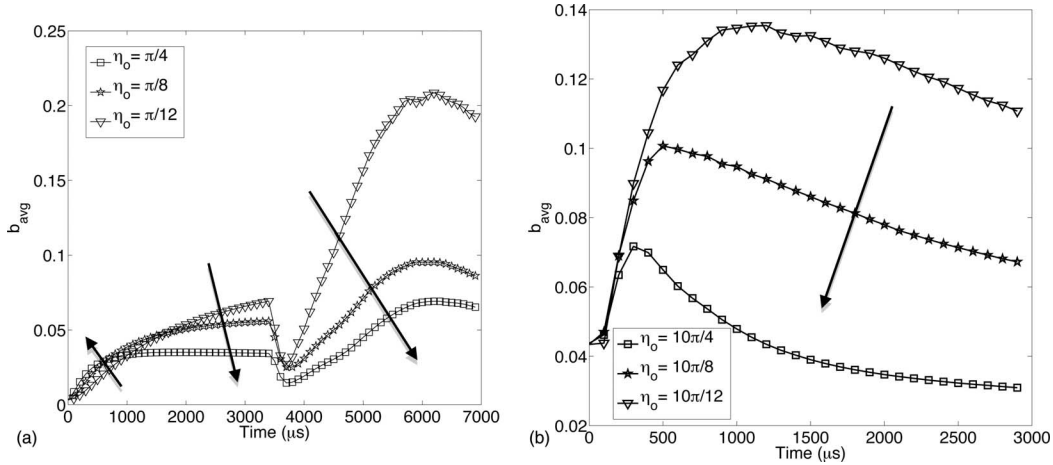
FIG. 17. The evolution of b_{avg}. (a) Low-η_o first shocked/reshocked; (b) high-η_o first-shocked only.

cross over and have higher second order moments because they have experienced less cumulative stirring, $\langle \rho'_{,i} S_{ij} \rho'_{,j} \rangle$, than the higher η_o cases and are not decaying as the cascade is not dissipating them as fast as the high η_o case—and consequently they have larger magnitudes before the reshock (see Figs. 17(a) and 18(a)). This does not occur for the enstrophy field (the dissipative mechanism for the kinetic energy) as its primary production mechanism for the low-η_o cases is baroclinic, i.e., it involves the source term $\varepsilon_{ijk}\langle \omega_i \rho_{,j} p_{,k} \rangle$, where ε_{ijk} is the Levi-Civita symbol, and not the usual nonlinear stretching term $\langle \omega_i S_{ij} \omega_j \rangle$ of the cascade, the analog to the stirring $\langle \rho'_{,i} S_{ij} \rho'_{,j} \rangle$. Framing the discussion of mixing in this way is peculiar to a moment closure approaches to turbulence, see Refs. 22 and 42 and references therein.

It is useful on many counts for modeling purposes, to examine the normalized density variance $\overline{\langle \rho'^2 \rangle}/\overline{\langle \rho^2 \rangle}$. In some second order closures,[37] an equation for the density variance is solved and in the mass flux equation the density intensity is taken as an approximation $b_{avg} \approx \overline{\langle \rho'^2 \rangle}/\overline{\langle \rho^2 \rangle}$—this is the leading Boussinesq approximation.[37] Interestingly, comparison of b_{avg} (Fig. 17) and $\overline{\langle \rho'^2 \rangle}/\overline{\langle \rho^2 \rangle}$ (Fig. 19) shows that they do behave qualitatively and almost quantitatively the same, and thus the approximation is useful for the statistics studied. Recall that both b and the density variance, as described above, are an ensemble average in the well mixed portions of the layer. While not the
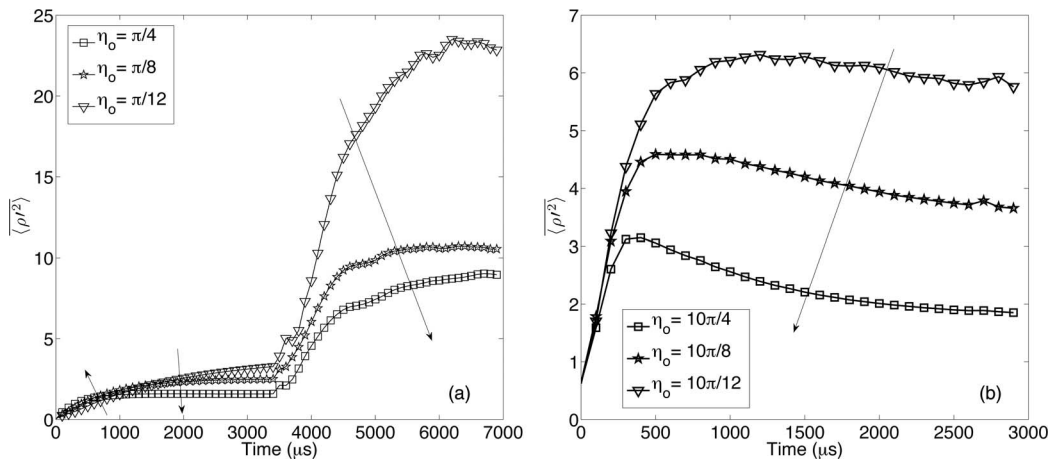

FIG. 18. Evolution of the mean mass-density variance $\overline{\langle \rho'^2 \rangle}$. (a) Low-$\eta_o$ first shocked/reshocked; (b) high-η_o first-shocked only.

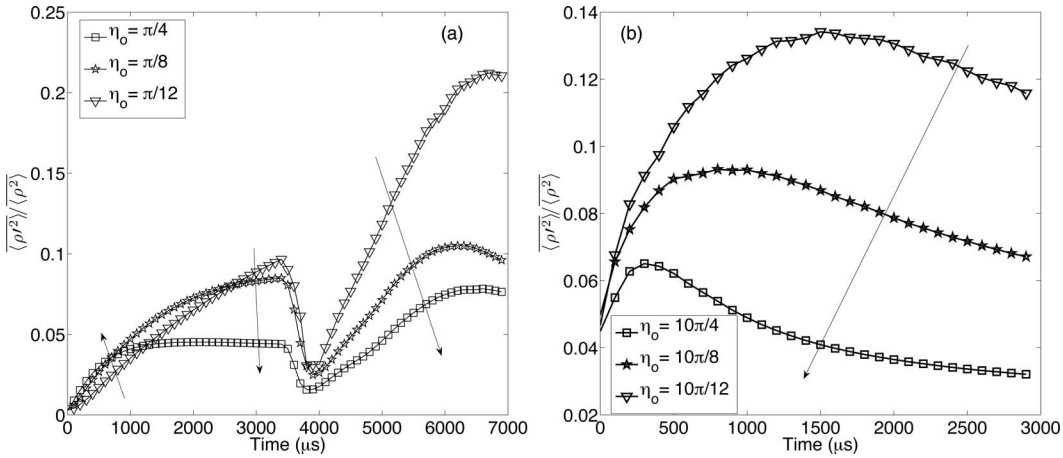FIG. 19. Evolution of $\overline{\langle \rho'^2 \rangle}/\overline{\langle \rho^2 \rangle}$. (a) Low-$\eta_o$: first shock and reshock; (b) high-η_o: first shock.

subject of our studies, we have seen that the approximation degrades substantially at the edges of the layer as might be anticipated by the Taylor series expansion of b given in Ref. 30. Results for the maximum value of b, which represent the least mixed extrema of the field, are given in Fig. 20. In all cases, there is a rise of the covariance with the impact of the shock, followed by their monotonic decay. In the fully mixed state $b = 0$.

Thus having discussed some of the moments that one might expect a turbulence model to predict, we move on to a discussion of the modeling challenges of these two classes of RMI instabilities and their dependence on ICs.

VI. CHALLENGES FOR MOMENT CLOSURE MODELS

The two very different shock-driven flow behaviors discussed above are relevant to the generality of turbulence models in predicting these classes of instabilities. The low-η_o case corresponds to impulsive acceleration of an almost-flat interface, the classical small-perturbation RMI. The high-η_o regime corresponds to: (a) impulsive acceleration of a very rough initial interface, and (b) shock passage through a turbulent material interface. It appears that simple models of RMI type flows cannot currently handle both classes of ICs (for a given initial A, Ma), and are certainly not likely to predict RMI flows with sequential shocks. We now highlight some unique flow physics that current
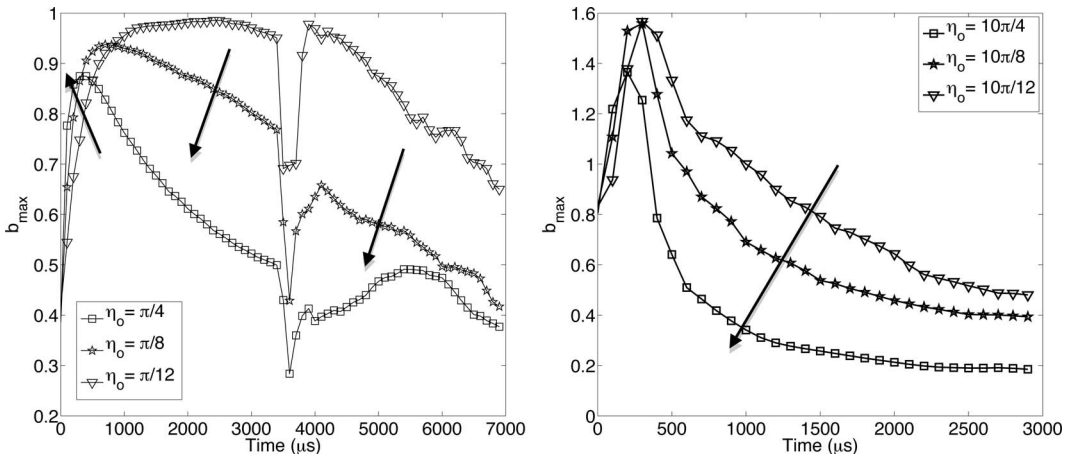

FIG. 20. Evolution of $b_{\max}$. (a) Low-η_o first shocked/reshocked; (b) high-η_o first-shocked only.

turbulence closure models – built as they are on self-similarity and equilibrium assumptions – are not likely to capture. The physically meaningful data to validate a moment closure against will be $\delta(t)$, $\delta(t)\dot{\delta}(t)$, K, and $K^{1/2}\,\delta(t)$—which are, respectively, the *rms* mixing layer thickness, a bulk *Re* proxy, the kinetic energy, and the turbulent eddy viscosity.

A. Challenge 1

Can one predict the temporal evolution of a quantity used in a moment closure for either the high-η_o or low-η_o class of the instability?

1. Scaling of the mixing layer thickness

Fig. 4 shows two distinct scalings for the mixing layer width for the high-η_o and low-η_o cases. If a moment closure is to capture the two instability behaviors it will have to capture the very different high-η_o ($\delta \sim t^{1/2}$) and low-η_o ($\delta \sim t$) scalings as well as trends. We speculate that most current models will fail as model development appears to have focused primarily on the equilibrium decay regime and use self-similarity.

2. Magnitude of shock response

The data indicate a very different response to the shock depending on the η_o, $\eta(t_{res})$, of the interface. For the high-η_o cases the four moment closure metrics and the dissipation $\varepsilon \sim \Omega$ are an order of magnitude or more larger than for the low-η_o ICs. This is an important difference.

B. Challenge 2

If one increases η_o within the high-η_o and low-η_o class of instabilities are the trends of the predicted quantities opposite of each other for K and δ and the same for Ω and b_{11}? In short, can a moment closure model be consistent with Eq. (6)?

1. Effects of initial rms slope on trends

As has been mentioned above and in Ref. 5 the RMI exhibits two very different behaviors depending on ICs which (for given initial A and Ma) are characterized by η_o (Eq. (6)).

2. Energy and enstrophy behave differently

At the passage of the shock across the high-η_o case, one finds, comparing Figs. 7–9, that the rise in kinetic energy and enstrophy do not track each other: the jump in K upon shock transit is the same for all the high-η_o cases while the jump in Ω differs by a factor of five between the highest η_o and lowest η_o examples of the high-η_o studies. Moreover (see Fig. 7) in the low-η_o case, K increases as η_o increases following a trend consistent with that predicted by the small perturbation theory of Richtmyer.[28] In the high-η_o case, K decreases as η_o is increased. In contrast, for both high and low η_o cases, the enstrophy increases. The production mechanisms of K and Ω are very different; in most turbulence models the production of enstrophy is modeled as proportional to the production of energy and these very different production terms likely need to be accurately modeled. To say that in another way: energy deposition and enstrophy deposition occur by different mechanisms. The current phenomenology in turbulence models cannot account for the difference in deposition.

Note that the figures show that the decay of K is different than the decay of Ω. Inspection of Fig. 7 shows that the higher the initial K (after shock time) the higher K is for the duration of the flow. While for enstrophy, the higher the initial Ω the lower it is by the end of the run as is seen in Fig. 8.

We have shown how the different RMI instabilities and their trends with initial *rms* interface slope are unlikely to be predicted with the standard form of models—the clearest difficulty being that such models, as currently configured, have built-in dependence on the *rms* slope either generally or as an initial condition input. We now look at implications of these typical model equations long after

the peak of the enstrophy and energy to understand whether these classes of models can compute a simple decay in our present (shock driven) context. We consider the moment equations long past the initial conditions and in the central portions of the now wide mixing zone, for which the modeled k and ε equations[40] for the decay are

$$\frac{1}{k}\frac{d}{dt}k \sim -\frac{\varepsilon}{k}, \quad \frac{1}{\varepsilon}\frac{d}{dt}\varepsilon \sim C_{\varepsilon 2}\frac{\varepsilon}{k}. \tag{7}$$

Based on the numerical simulation data averaged over the region M > 0.75 we compute the variables in the above equations. The objectives are the following: (1) to verify whether the form of the Eq. (7) will predict the different temporal trajectories of K and Ω, and (2) to verify the accepted wind tunnel value of the decay coefficient $C_{\varepsilon 2} = 1.33$. Our analysis (details not shown here) demonstrates that the above form of the decay equations does capture the trajectories of K and Ω. Moreover, we also take the ratio of the two Eq. (7) in order to compute the coefficient $C_{\varepsilon 2}$ based on the simulation data and find a robust $C_{\varepsilon 2} \approx 1.33$ for all the high-η_o cases and after reshock. For the low-η_o cases there is some variability but 1.33 serves usefully as a mean. With the decay coefficient being so close to conventional values (with some caveats for the low-η_o simulations) we conclude that the decay phase can be well modeled by the traditional phenomenology provided the flow is in the turbulent regime. Such an agreement is not to be expected: the model equations for the decay phase are built using wind tunnel turbulence phenomenology and not shock driven turbulence for which enstrophy and energy deposition by baroclinic processes are vastly different. Such agreement is not to be expected: the model equations for the decay phase are built using wind tunnel turbulence phenomenology and not shock driven turbulence for which enstrophy and energy deposition by baroclinic processes are vastly different.

3. Turbulent eddy viscosity

As mentioned above, in equilibrium turbulence, the spectral bandwidth and the turbulent Re have all been used as a measure of the nonlinear nature of the flow.[16, 17] Due to our interest in moment closure methods, we use the turbulent eddy viscosity as a proxy of these measures; recall that the fluid viscosity does not appear (in any important way) in moment closure methods for developed turbulence (away from walls). To this end we use the turbulent eddy viscosity $K^{1/2}\,\delta(t)$ as a metric of nonlinearity easily obtained from a moment closure calculation. Figure 13 shows very distinct behaviors of this quantity for the low-η_o and high-η_o and reshocked cases.

4. The anisotropy

Unlike the energy and mixing width the isotropy increases with increasing η_o in all cases (see Fig. 9).

VII. SUMMARY AND CONCLUSIONS

We have studied, for fixed Ma and A, how the initial rms interface slope affects the fluid and mixing physics of the RMI. We have observed the appearance of two different RM instabilities with distinctly different physics depending on the initial morphology of the air-SF_6 interface. Our study is a single parameter study, and has not studied the effects of varying A or Ma in order to study the interfacial morphology effects. Our findings are thus pertinent to the L-H first-shocked and the H-L reshocked interfaces as the initial A is kept fixed.

For fixed $A > 0$ and Ma, the rms slope of the initial material interface η_o appears to be a very important parameter in determining whether statistical trends are in a linear regime scaling as suggested by Richtmyer's model,[28] or in a nonlinear mode-coupled regime exhibiting many of the phenomenological characteristics of a cascade process producing additional small scales. The trends in these two regimes, as indicated by the response of the RMI to an increase in the rms slope of the interface, η_o, on the first-shocked L-H interface are opposite. The two identified RMI flow types can

be summarized with the following heuristic (Eq. (6)):

$$low-\eta_o, \quad \delta \sim t : \quad as \; \eta_o \uparrow \quad \Omega \uparrow \quad b_{11} \downarrow \quad K \uparrow \quad \delta \uparrow,$$
$$high-\eta_o, \quad \delta \sim t^{1/2} : \quad as \; \eta_o \uparrow \quad \Omega \uparrow \quad b_{11} \downarrow \quad K \downarrow \quad \delta \downarrow.$$

In the low-η_o case the baroclinic generation is the primary production mechanism for enstrophy. In the high-η_o case enstrophy is additionally and importantly generated by the amplification of vorticity interacting with the strain field as is characteristic of nonlinear mode coupling and the appearance of a cascade and smaller scales of the flow. The subsequent decay of the flow has many of the features of a decaying turbulent flow. The low-η_o case is consistent with the idea of little mode coupling and a linear growth ($\delta \sim t$) whose trends are consistent with the small perturbation impulse theory of Richtmyer.[28] This is the case of a first-shocked L-H interface on a relatively smooth interface. The first-shocked L-H high-η_o case is consistent with the idea of a nonlinearly mode-coupled flow with diffusive growth law ($\delta \sim t^{1/2}$).

The remarkable thing is that the increase in enstrophy that accompanies the increase in η_o for both high-η_o and low-η_o (first-shocked-L-H and first-shocked-L-H/reshocked-H-L) cases leads to two very different fluid dynamical responses: in the low-η_o case the kinetic energy increases associated with higher deposition of energy while in the high-η_o "nonlinear" (and reshocked) case there is a rapid production of new smaller scale motions and enstrophy and a large reduction in kinetic energy accomplished by a cascade mechanism. We have also observed these behaviors in our double interface (shocked gas-curtain) studies.[26] We have called this the *bipolar behavior* of the RMI and have shown that two very distinct classes of fluid physics appear in the RMI configuration.

Our current presentation and previous results[21, 26] have used a single-parameter η_o (for fixed *Ma*, *A*) to discuss IC dependence of the trends in the fluid and mixing physics of shock-driven transition and the appearance of two different instabilities. In no way should this be interpreted as a statement that we believe that the IC problem can be characterized by a single parameter. We merely report on identifying one way of diagnosing and presenting the diversity of the early and intermediate time RMI which may provide an effective framework to assess the performance of reduced-order turbulence closure models. The material interface instabilities, as seen in the short and intermediate time mixing-layer response to a shock, likely have a very complicated dependence on many other relevant variables and various proposals are being explored, e.g., Refs. 18 and 20.

The first-shocked L-H high-η_o results when contrasted to the low-η_o first-shocked L-H studies support the idea that RMI can go directly to a nonlinear mode coupled flow state producing more small scales on the first shock with high enough η_o. The reshocked H-L low-η_o case has the same ordering of trends with *rms slope* $\eta(t_{res})$, at the time of the reshock as the first-shocked L-H high-η_o case. The $\eta(t_{res})$ at the initiation of the H-L reshock is in the nonlinear regime and the trends with increasing $\eta(t_{res})$ at initiation of the H-L reshock are consistent with the η_o trends in the high-η_o case first-shock L-H. Given that the same trends with $\eta(t_{res})$ are seen for the H-L reshock case as in the high-η_o first-shock L-H case one speculates that the reshock goes directly to a nonlinear mode coupled flow and cascade by the same mechanism as the nonlinear first-shock case. As the primary generation of vorticity for high $\eta(t_{res})$ and η_o is the nonlinear cascade and not baroclinicity we believe that these trends will be also seen in $A < 0$ simulations—but until this can be confirmed it remains an open question.

The fact that slower growth rate of the high-η_o mixing-layer width is associated with more material mixing—contrary to intuition at first glance, demonstrates that mixing-layer width growth-rate, bulk *Re*, and material mixing are not causally connected. Our observations have a very straightforward physical explanation: higher initial material interface slope leads to production of more smaller scales which dissipate turbulent kinetic energy faster, reducing the layer growth rate and increasing the mixing rate—in short higher mixing-layer width growth rate does not mean more (molecular) mixing. We showed that the first-shocked high-η_o case has very different trend scalings than first shocked low-η_o case. The two very different RMI behaviors are relevant to the generality of models used to predict these classes of flows. Current statistical model strategies cannot distinguish between these two classes of flows.

ACKNOWLEDGMENTS

[1] M. Brouillette, "The Ritchmyer-Meshkov instability," Annu. Rev. Fluid Mech. **34**, 445–468 (2002).

[2] S. Balasubramanian, G. C. Orlicz, K. P. Prestridge, and B. J. Balakumar, "Experimental study of initial condition dependence on Richtmyer-Meshkov instability in the presence of reshock," Phys. Fluids **24**, 034103 (2012).

[3] J. W. Jacobs and J. M. Sheeley, "Experimental study of incompressible Richtmyer- Meshkov instability," Phys. Fluids **8**, 405–415 (1996).

[4] M. Vetter and B. Surtevant, "Experiments on the Richtmyer–Meshkov instability of an air/ SF_6 interface," Shock Waves **4**, 247–252 (1995).

[5] F. Poggi, M. H. Thorembey, and G. Rodriguez, "Velocity measurements in turbulent gaseous mixtures induced by Richtmyer-Meshkov instability," Phys. Fluids **10**, 2698 (1998).

[6] E. Leinov, G. Malamud, Y. Elbaz, A. Levin, G. Ben-dor, D. Shvarts, and O. Sadot, "Experimental and Numerical Investigation of the Richtmyer–Meshkov Instability under reshock conditions," J. Fluid Mech. **626**, 449–475 (2009).

[7] R. L. Holmes, G. Dimonte, B. Fryxell, M. L. Gittings, J. W. Grove, M. Schneider, D. H. Sharp, A. L. Velikovich, R. P. Weaver, and Q. Zhang, "Richtmyer–Meshkov instability growth: Experiment, simulation and theory," J. Fluid Mech. **389**, 55–79 (1999).

[8] R. H. Cohen, W. P. Dannevik, A. M. Dimits, D. E. Eliason, A. A. Mirin, Y. Zhou, D. H. Porter, and P. R. Woodward, "Three-dimensional simulation of a Richtmyer–Meshkov instability with a two-scale initial perturbation," Phys. Fluids **14**, 3692–3709, (2002).

[9] J. A. Greenough and E. Burke, "The effect of initial conditions on late time asymptotics and mixing for multimode Richtmyer–Meshkov instability," in *Proceedings of the 9th International Workshop on the Physics of Compressible Turbulent Mixing*, Cambridge, UK, 19–23 July 2004.

[10] D. J. Hill, C. Pantano, and D. I. Pullin, "Large-eddy simulation and multiscale modeling of a Richtmyer–Meshkov instability with reshock," J. Fluid Mech. **557**, 29–61 (2006).

[11] D. L. Youngs, "Rayleigh–Taylor, and Richtmyer–Meshkov mixing," in *Implicit Large Eddy Simulation: Computing Turbulent Fluid Dynamics*, 2nd printing, edited by F. F. Grinstein, L. G. Margolin, and W. J. Rider (Cambridge University Press, 2010), Chap. 13.

[12] O. Schilling and M. Latini, "High-order WENO simulations of three-dimensional reshocked Richtmyer–Meshkov instability to late times: Dynamics, dependence on initial conditions, and comparisons to experimental Data," Acta Math. Sci. **30B**(2), 595–620 (2010).

[13] B. Thornber, D. Drikakis, R. J. R. Williams, and D. L. Youngs, "The influence of initial conditions on turbulent mixing due to Richtmyer-Meshkov instability," J. Fluid Mech. **654**, 99–139 (2010).

[14] F. F. Grinstein, A. A. Gowardhan, and A. J. Wachtor, "Simulations of Richtmyer-Meshkov instabilities in planar shock-tube experiments," Phys. Fluids **23**, 034106 (2011).

[15] M. Hahn, D. Drikakis, D. L. Youngs, and R. J. R. Williams, "Richtmyer–Meshkov turbulent mixing arising from an inclined material interface with realistic surface perturbations and reshocked flow," Phys. Fluids **23**, 046101 (2011).

[16] B. Thornber, D. Drikakis, D. L. Youngs, and R. J. R. Williams, "Growth of a Richtmyer-Meshkov turbulent layer after reshock," Phys. Fluids **23**, 095107 (2011).

[17] B. Thornber, D. Drikakis, D. L. Youngs, and R. J. R. Williams, "Physics of the single-shocked and reshocked Richtmyer–Meshkov instability," J. Turbul. **13**, N10, 1–17 (2012).

[18] M. Lombardini, D. J. Hill, D. I. Pullin, and D. I. Meiron, "Atwood ratio dependence of Richtmyer–Meshkov flows under reshock conditions using large-eddy simulations," J. Fluid Mech. **670**, 439–480 (2011).

[19] S. Ukai, K. Balakrishnan, and S. Menon, "Growth rate predictions of single- and multi-mode Richtmyer–Meshkov instability with reshock," Shock Waves **21**, 533–546 (2011).

[20] K. O. Mikaelian, "Extended model for Richtmyer-Meshkov mix," Physica D **240**, 935–942 (2010).

[21] A. A. Gowardhan, J. R. Ristorcelli, and F. F. Grinstein, "The bipolar behavior of the Richtmyer-Meshkov instability," Phys. Fluids **23**, 071701 (2011).

[22] H. Tennekes and J. L. Lumley, *A First Course in Turbulence* (MIT Press, Cambridge, MA, 1972).

[23] *Implicit Large Eddy Simulation: Computing Turbulent Flow Dynamics*, 2nd printing, edited by F. F. Grinstein, L. G. Margolin, and W. J. Rider (Cambridge University Press, New York, 2010).

[24] A. J. Wachtor, F. F. Grinstein, C. R. Devore, J. R. Ristorcelli, and L. G. Margolin, "Implicit large-eddy simulations of passive scalar mixing in statistically stationary isotropic turbulence," Phys. Fluids **25**, 025101 (2013).

[25] M. Gittings, R. Weaver, M. Clover, T. Betlach, N. Byrne, R. Coker, E. Dendy, R. Hueckstaedt, K. New, W. R. Oakes, D. Ranta, and R. Stefan, "The RAGE radiation-hydrodynamic code," Comput. Sci. Discov. **1**, 015005 (2008).

[26] A. A. Gowardhan and F. F. Grinstein, "Numerical simulation of Richtmyer–Meshkov instabilities in shocked gas curtains," J. Turbul. **12**, N43, 1–24 (2011).

[27] K. R. Sreenivasan, A. Prabhu, and R. Narasimha, "Zero-crossings in turbulent signals," J. Fluid Mech. **137**, 251–272 (1983).

[28] R. D. Richtmyer, "Taylor instability in shock acceleration of compressible fluids," Commun. Pure Appl. Math. **13**, 297–319 (1960).

[29] A. Cook and P. Dimotakis, "Transition stages of the Rayleigh Taylor instability between miscible fluids," J. Fluid Mech. **443**, 69–99 (2002).

[30] D. L. Livescu, J. R. Ristorcelli, R. A. Gore, S. H. Dean, W. H. Cabot, and A. Cook, "High-Reynolds number Rayleigh-Taylor turbulence," J. Turbul. **10**, N13, 1–32 (2009).

[31] Y. Zhou, "Unification and extension of the similarity scaling criteria and mixing transition for studying astrophysics using high energy density laboratory experiments or numerical simulations," Phys. Plasmas **14**, 082701 (2007).

[32] P. E. Dimotakis, "The mixing transition in turbulent flows," J. Fluid Mech. **409**, 69–98 (2000).

[33] G. C. Orlicz, B. J. Balakumar, C. D. Tomkins, and K. P. Prestridge, "A Mach number study of the Richtmyer-Meshkov instability in a varicose heavy gas curtain," Phys. Fluids **21**, 064102 (2009).

[34] J. L. Lumley, "Computational modeling of turbulent flows," Adv. Appl. Mech. **18**, 123–176 (1979).

[35] W. K. George, "The decay of homogeneous isotropic turbulence," Phys. Fluids A **4**(7), 1492–1509 (1992).

[36] P. G. Saffman, "Large-scale structure of homogeneous turbulence," J. Fluid Mech. **27**(3), 581 (1967).

[37] O. Grégoire, D. Souffland, and S. Gauthier, "A second-order turbulence model for gaseous mixtures induced by Richtmyer–Meshkov instability," J. Turbul. **6**, N29, 1–20 (2005).

[38] J. R. Ristorcelli and N. Hjelm, "Initial moments and parameterizing transition for Rayleigh-Taylor unstable stochastic interfaces," J. Turbul. **11**, N46, 1–27, (2010).

[39] L. Skrbek and S. R. Stalp, "On the decay of homogeneous isotropic turbulence," Phys. Fluids **12**, 1997–2019 (2000).

[40] S. B. Pope, *Turbulent Flows* (Cambridge University Press, 2000).

[41] J. D. Schwarzkopf, D. Livescu, R. A. Gore, R. M. Rauenzahn, and J. R. Ristorcelli, "Application of a second-moment closure model to mixing processes involving multi-component miscible fluids," J. Turbul. **12**, N49, 1–35 (2011).

[42] J. R. Ristorcelli, "Passive scalar mixing: Analytic study of time scale ratio, variance, and mix rate," Phys. Fluids **18**, 075101 (2006).